Non-affine deformation in microstructure selection in solids: I. Molecular dynamics

2008 J. Phys.: Condens. Matter 20 365210

(http://iopscience.iop.org/0953-8984/20/36/365210)

J. Phys.: Condens. Matter **20** (2008) 365210 (7pp) doi:10.1088/0953-8984/20/36/365210

Non-affine deformation in microstructure selection in solids: I. Molecular dynamics

Jayee Bhattacharya[1], **Arya Paul**[1], **Surajit Sengupta**[1] **and Madan Rao**[2,3]

[1] S N Bose National Centre for Basic Sciences, Block JD, Sector III, Salt Lake, Calcutta 700 098, India
[2] Raman Research Institute, C V Raman Avenue, Bangalore 560 080, India
[3] National Centre for Biological Sciences (TIFR), Bellary Road, Bangalore 560 065, India

Received 1 May 2008
Published 14 August 2008
Online at stacks.iop.org/JPhysCM/20/365210

Abstract

We study the nucleation dynamics and microstructure selection in a model two-dimensional solid undergoing a square to rhombic transformation, using coarse-grained molecular dynamics (MD) simulations. We find a range of microstructures depending on the depth of quench. The transformations are accompanied by the creation of transient and localized *non-affine zones* (NAZ), which evolve with the rapidly moving parent–product interface. These plastic regions are created beyond a threshold stress, at a rate proportional to the local stress. We show that the dynamics of NAZs determines the selection of microstructure, including the ferrite and martensite.

(Some figures in this article are in colour only in the electronic version)

1. Introduction

The dynamics following a quench across a solid state structural transition rarely takes the solid to its equilibrium state [1]. Severe dynamical constraints experienced by the product *inclusion* within the parent crystal determine the mode of nucleation and of subsequent growth. Often, solids get stuck in long-lived *microstructures*, which depend on the depth of quench and cooling rate [2]. For example, transformations occurring at high temperatures are typically accompanied by large-scale rearrangements of atoms; in this case the elasticity of the solid plays only a minor role in determining the microstructure. On the other hand, at low temperatures, only local rearrangements of atoms are possible; the resulting microstructures are largely determined by elasticity [3]. These are just two of the myriad possibilities explored by the transforming solid. Which of these is actually selected, i.e. can we construct a dynamical phase diagram for microstructure?

In a set of papers [4–6], we had explored these issues in the context of a model solid undergoing a two-dimensional square to rhombic structural transformation. We found that, when the transformation proceeds at a high temperature, the resulting product nucleus is isotropic and polycrystalline, while a low transformation temperature induces the formation of an anisotropic nucleus, roughly elliptical, consisting of a pair of twin-related crystallites [6]. The two modes of nucleation may be denoted *ferrite* and *martensite*, borrowing terminology from the microstructure of steel [1]. By following the nucleation dynamics in 'microscopic' detail, we had established that the ferrite nucleus is formed following extensive rearrangements of atomic coordinates, while the martensite nucleus follows from a transformation where the local connectivity of the lattice is, to a large extent, preserved. This is consistent with the two paradigms commonly described in real materials. However, these two limits are not mutually exclusive; indeed, for intermediate temperatures, the transformation proceeds such that both mechanisms may operate at different spatial and temporal locations, a feature observed in real materials [7]. Further, the different microstructures (twinned and untwinned) were obtained simply by tuning appropriate kinetic parameters.

Our preliminary attempts at a unifying picture [6] were based on the recognition (from the MD simulation) of the role played by *non-elastic* variables, which we identified with local density fluctuations. We showed that the coupled dynamics of density fluctuations and elastic strain determined the microstructure of the growing nucleus. In this, and in a companion paper [8] we provide a more refined understanding of solid state nucleation and microstructure selection. Part I of a set of two papers deals with the results of our extensive

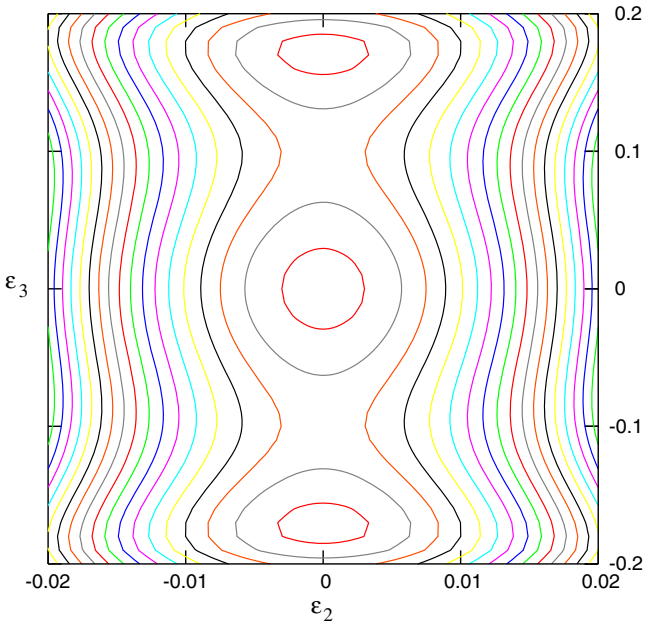

Figure 1. Contour plot of the zero-temperature energy per particle for $\rho = N/V = 1.05, \alpha = 1$ and $v_3 = 0.204$ as a function of the OP strains (e_2, e_3) showing a metastable square minimum at $(0, 0)$ and two degenerate, stable rhombic (*oblique*) minima at $(0, \pm 0.18)$.

MD simulations: we show that *internal stresses* generated during the transformation create local *non-affine zones* (NAZ) beyond a threshold stress. We find that the dynamics of these NAZs determines the selection of the microstructure. We then highlight four generic principles derived from our MD simulations and use these to construct an elastoplastic theory for the dynamics of solid state transformations, the subject of part II.

The rest of this paper is organized as follows. In the next section, we describe our model solid and our MD simulations on the square to rhombic transition. In section 3 we present our results with special emphasis on the identification of NAZs and their evolution during the solid state transformation. We show that our results may be distilled into a set of principles which underlie microstructure selection in our model. We end the paper with a summary and conclusion in section 4.

2. The coarse-grained model and molecular dynamics simulations

A simple effective model which shows transitions between square and rhombic (a special case of the more general *oblique*) lattices comprises of particles which interact via the potential [5, 6]

$$1/2 \sum_{i \neq j} V_2(\mathbf{r}_{ij}) + 1/6 \sum_{i \neq j \neq k} V_3(\mathbf{r}_i, \mathbf{r}_j, \mathbf{r}_k), \qquad (1)$$

where $\mathbf{r}_i$ is the position vector of particle i and $r_{ij} \equiv |\mathbf{r}_{ij}| \equiv |\mathbf{r}_j - \mathbf{r}_i|$. The *anisotropic* two-body potential [5] is purely repulsive and short ranged:

$$V_2(\mathbf{r}_{ij}) = v_2 \left(\frac{\sigma_0}{r_{ij}}\right)^{12} \{1 + \alpha \cos^2 2\theta_{ij}\} \qquad (2)$$

where σ_0 and v_2 set the units of length and energy, α is an 'anisotropic lock-in' parameter [5] and θ_{ij} is the angle between $\mathbf{r}_{ij}$ and an arbitrary external axis. The short-ranged three-body interaction [9]

$$V_3(\mathbf{r}_i, \mathbf{r}_j, \mathbf{r}_k) = v_3 \left[f_{ij} f_{jk} \sin^2 4\theta_{ijk} + \text{permutations} \right], \qquad (3)$$

where the function $f_{ij} \equiv f(r_{ij}) = (r_{ij} - r_0)^2$ for $r_{ij} < r_0 = 1.8\sigma_0$ and 0 otherwise and the angle θ_{ijk} is the angle between the vectors $\mathbf{r}_{ij}$ and $\mathbf{r}_{jk}$. The two-body and three-body interactions favor rhombic and square ground states, respectively. Inclusion of the two-body anisotropic lock-in parameter α is a device to vary the jump in the order parameter from strongly first order ($\alpha = 0$) to a continuous transition for $v_3 = 0, \alpha \sim 1.5$.

The rhombic lattice is a special case of the general oblique lattice—one of the five possible two-dimensional Bravais lattices. In general, we need two order parameters (OP) to describe the transition between square and oblique lattices, i.e. between the space groups $p4mm \rightarrow p2$. Noting that the affine strain tensor $\epsilon_{ij} = \mathbb{T}_{ij} - \delta_{ij}$ (δ_{ij} is the Kronecker tensor) and i and $j = 1, 2$ (or x, y); these are the affine shear strain $e_3 = \epsilon_{xy} = \epsilon_{yx}$ and the deviatoric strain $e_2 = (\epsilon_{xx} - \epsilon_{yy})$. Thus from symmetry considerations alone, we would expect to obtain four symmetry-related product phases [10]. However, the microscopic model used by us obtains a rhombic lattice for which e_2 identically vanishes and the four equivalent variants merge in pairs to give *two* symmetry-related products. To show this we have plotted in figure 1 the $T = 0$ energy obtained for our model solid with the parameters $\alpha = 1, v_3 = 0.2$ and at $\rho = 1.05$ for various values of e_2 and e_3, taking the square lattice as the reference. Apart from the minimum corresponding to the square lattice we obtain only two other minima representing the two rhombic variants. The value of e_2 at all the three minima is zero. It is therefore sufficient to use e_3 as the sole order parameter (OP) for this transition. When the anisotropic parameter $\alpha = 0$, the product rhombic lattice is close to being triangular, corresponding to a strongly first-order structural transition with a large jump in the OP ($\Delta e_3 \sim \pm .3$) and a relatively large volume change [5, 6]. This jump in the OP at the structural transition can be made arbitrarily small by taking $\alpha > 0$ [5]; our qualitative results are exactly the same, as long as $\Delta e_3 > 0$ at the transition.

The unit of time in our simulations is $\sigma_0\sqrt{m/v_2}$, where m is the particle mass. Using typical values, this translates to an MD time unit of 1 ps. Knowing the individual-particle MD trajectories allows us to project time-dependent atomic positions into time-varying coarse-grained *fields* (e.g. e_1, e_3, etc) whose evolution can be monitored during the transformation.

Both the two- and three-body potentials are purely repulsive and therefore the system needs to be confined either in a box of fixed volume or by an external compression [11]. In this paper, we discuss our results for MD simulations in the constant number, volume (and shape) and temperature (NVT) ensemble with periodic boundary conditions using a Nosé–Hoover thermostat. We have, in addition, carried out extensive simulations in the constant stress ($N\Sigma T$) ensemble with open boundaries using an additional confining potential which, at

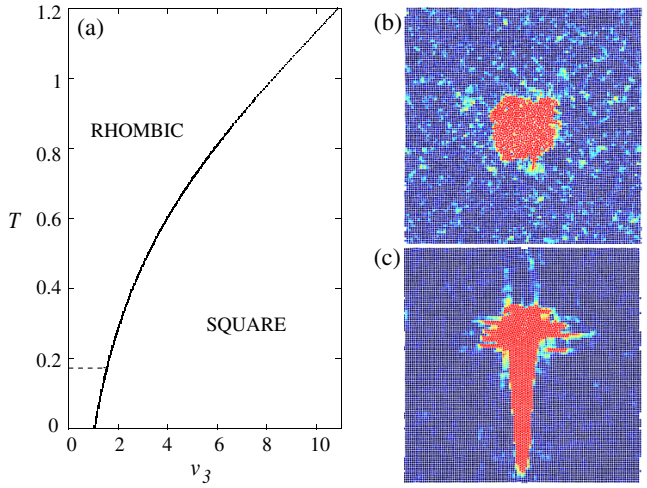

Figure 2. (a) Phase diagram in the T–v_3 plane (with $\alpha = 0$): the solid line is the phase boundary between square and rhombic crystals. The dashed line marks the temperature above which anisotropic, twinned nuclei become rare and is identified as the martensite start (or M_s) temperature [1] for our model. Typical product nuclei formed following quenches at (b) $T = 0.8$ ($v_3 = 10 \rightarrow 5.5$) to obtain the isotropic 'ferrite' and (c) $T = 0.1$ ($v_3 = 5 \rightarrow 1.65$) to obtain the anisotropic, twinned martensite, starting with an equilibrated square parent crystal composed of 12 099 particles.

the same time, allows for changes of the overall shape of the crystal during the transformation. Our main results concerning the dynamics and mechanism of microstructure selection are the same in both the ensembles. A detailed comparison of MD simulation of our model system in various ensembles, starting from a variety of initial states and for the full range of the potential parameters is being prepared for publication elsewhere.

The equations of motion for up to $N = 20\,000$ particles are integrated using a Verlet scheme [11] with a time step $\Delta t = 10^{-3}$. The relaxation time of the Nosé–Hoover thermostat [11] Q determines how fast the system relaxes to the ambient temperature. Equilibrium properties are unaffected by this parameter, which is chosen to produce fast relaxation, at the same time avoiding numerical instabilities. On the other hand, dynamical properties can be sensitive to this parameter. However, our results are robust to changes of Q within reasonable limits.

An accurate equilibrium phase diagram of the system (figure 2) in the T–v_3 plane for density $\rho_0 = N/V = 1.1$ is obtained by computing and comparing the free energies of square and rhombic lattices using the technique outlined in [12].

3. Results: dynamics of nucleation and growth

We shall now describe our results for a study of the nucleation dynamics of a solid in solid, following a quench across the structural transition. Our effort will be to extract general matters of principle from these simulations; we will highlight these as we go along.

A typical quench from a square to a rhombic solid into a region where the square lattice is metastable initiates multiple nucleation events (at least at high temperatures), making a quantitative analysis of the dynamics of a single critical nucleus cumbersome. We get over this difficulty by introducing a nucleation seed at the center of the simulation box. The seeding consists of replacing the central particle with a particle whose size σ is smaller by a factor $\delta \equiv (\sigma_0 - \sigma)/\sigma_0$. We have taken $0.25 \leqslant \delta \leqslant 1$, so as to obtain nucleation events within reasonable computation time. Having equilibrated the seeded square crystal at large v_3, we 'quench' across the phase coexistence line by varying the coefficient of the three-body term v_3 at two different temperatures $T = 0.8$ and 0.1. While the seeding is a matter of convenience at the higher temperature, it is necessary at the lower temperature. The transformation at the lower temperature proceeds via heterogeneous nucleation [6].

In figures 2(b) and (c), we show a snapshot of the resulting microstructure following a quench from the equilibrated square lattice at temperatures $T = 0.8$ and 0.1, respectively. The colors indicate the local bond-angle order parameter which is defined to vary from 0 (blue) in the square lattice to 1 (red) in the rhombic [6]. It is clear from the particle position snapshots, figures 2(b) and (c), that the product nucleus is isotropic for large temperatures and highly anisotropic for small temperatures. We identify the isotropic nucleus with a *ferrite* and the anisotropic one with *martensite* [6]. This identification is reinforced by showing that the latter is twinned.

(1) Solid state transformations predominantly proceed via nucleation. At low temperatures, the nucleation of the product solid is heterogeneous and is initiated by 'seeding' the parent.

To follow the dynamics in quantitative detail, we compute the coarse-grained local strain field using the procedure introduced in [13]. Briefly, we compare the immediate neighborhood Ω, centered around $\mathbf{r}$, of any tagged particle 0 (defined using a cutoff distance equal to the range of the potential) in the initial, reference, lattice (at time $t = 0$) with that of the same particle in the transformed lattice. We obtain the 'best-fit' local affine strain ϵ_{ij} which maps as nearly as possible all the particles n in Ω from the reference to the transformed lattice using an affine connection. This is done by minimizing the (positive) scalar quantity:

$$D^2_\Omega(\mathbf{r}, t) = \sum_{n\in\Omega}\sum_i \Bigg\{ r^i_n(t) - r^i_0(t) - \sum_j (\delta_{ij} + \epsilon_{ij}) \times (r^j_n(0) - r^j_0(0)) \Bigg\}^2 \quad (4)$$

with respect to choices of affine ϵ_{ij}. Here, again, the indices i and $j = x, y$, and $r^i_n(t)$ and $r^i_n(0)$ are the ith component of the position vector of the nth particle in the reference and transformed lattice, respectively. Any *residual* value of $D^2_\Omega(\mathbf{r}, t)$ is a measure of *non-affineness*.

Figure 3(a) shows the nucleation and growth of the twinned martensite nucleus, following the lower temperature quench—we have plotted the best-fit e_3 for snapshot configurations of $N = 110 \times 110$ particles at time steps of 2000, 3000, 4000 and $5000\Delta t$. The twinned structure of the nucleus composed of the two degenerate rhombi (characterized by positive and negative values of e_3, separated by a sharp

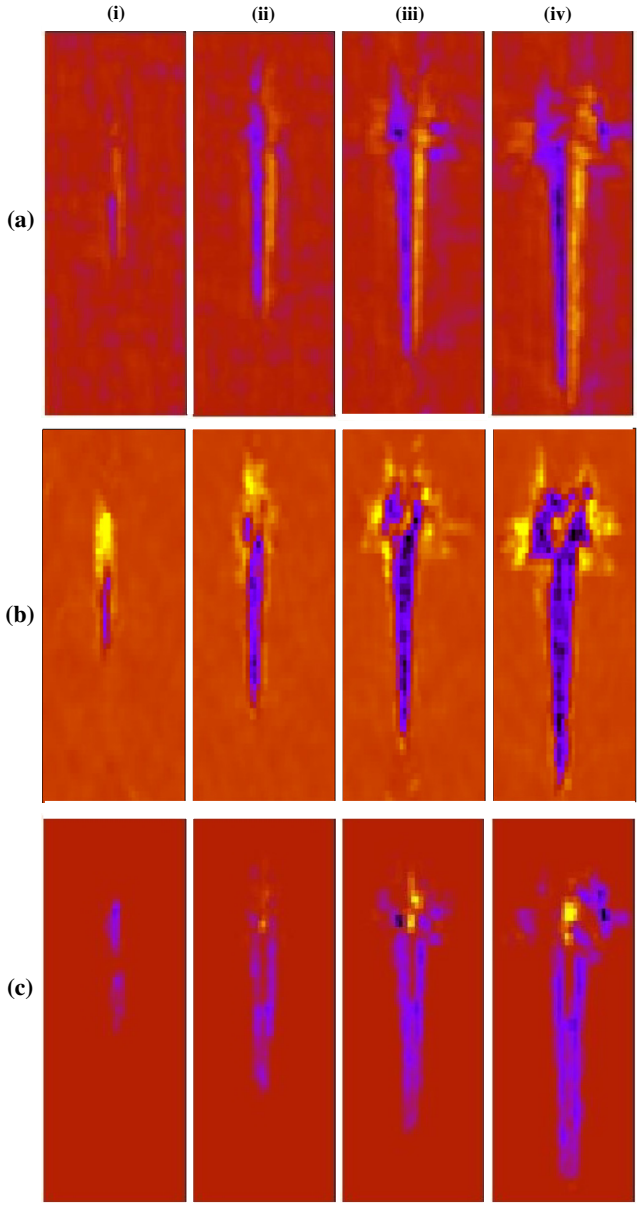

Figure 3. Best-fit affine strains and residual non-affine deformations, obtained from MD simulations of particles undergoing a square to rhombic transition at $T = 0.1$, for time slices (i) 2000, (ii) 3000, (iii) 4000 and (iv) $5000\Delta t$. Plots obtained by coarse-graining the $N = 110 \times 110$ lattice to a 64×64 lattice. (a) Order parameter (shear) strain e_3, colors show e_3 from -0.3 (black) to 0 (brown/gray in the print edition) to 0.3 (yellow/white in the print edition). The twinned microstructure is clearly visible, even at earlier times. (b) Non-order parameter (volumetric) strain e_1, colors show e_1 from -0.5 (black) to 0.3 (yellow/white in the print edition). The equilibrium value of e_1 is nonzero within the rhombic phase. In addition, e_1 appears at the two ends of the twinned microstructure due to elastic coupling to the order parameter e_3. (c) Non-affine deformation χ. Colors show χ ranging from -1 to 1. Note that $\chi \to 0$ at the center of the growing nucleus at large times. The NAZs surround the growing nucleus and are created at and advected by the front. Jammed and unjammed NAZs occur at the 'top' and 'bottom' of the nucleus, respectively, sharing the same spatial symmetries as e_1.

boundary) is evident even at the earliest time, and becomes more pronounced as time progresses. The constraint of fixed density forces a dynamical coupling between the affine OP strain and the affine non-order parameter (NOP) volume strain $e_1 = \epsilon_{xx} + \epsilon_{yy}$, so that the transformation is also accompanied by a volume change, figure 3(b). As a result, as the transformation proceeds, more and more particles are pushed up against the surrounding untransformed square lattice which creates a *jammed* region at one end and an *unjammed* region at the other end of the anisotropic martensitic nucleus, figure 3(b).

(2) The dynamics of transformation is described by an affine OP strain (here, shear strain) characterizing the microstructure of the growing nucleus, and an affine NOP strain (here, volumetric strain), which is slaved to the former.

We can now use the residual D^2_Ω (4) to extract the spatio-temporal variation of any non-affine deformation that is produced during the transformation. To be able to distinguish between non-affineness arising from different components of the strain (shear or volumetric) distortion, we need to incorporate the notion of jamming in the definition of non-affineness (4). In the context of granular compaction [14] and glassy materials [15], jamming has been quantified in terms of changes in the local free volume relative to the reference state. In our context, this translates into computing the relative change in the distance between particles within Ω in the direction of motion of the particles in the nucleus, denoted by Δl; we may thus define a quantity $\chi(\mathbf{r}, t) = -D^2 \operatorname{sgn}(\Delta l)$, which takes both positive (jammed) and negative (unjammed) values. For the martensite nucleus, the jammed and unjammed non-affine zones (NAZs) are shown in figure 3(c); as the transformed region grows, χ is localized and advected by the transformation front. Note that the spatial symmetries of χ are the same as that of e_1 at all times (compare figures 3(b) and (c)), and so we associate the non-affineness predominantly with the NOP or volumetric strain. This restriction of non-affineness to the NOP strain alone could be specific to the square-to-rhombus transition; in transitions between other structures, there could be a fair degree of plasticity associated with the OP strain too. We will return to this point in [8]. Consistent with geometrical theories, the NAZs are absent at the twin interface; this interface is coherent and the twins are simply related to each other by an affine transformation.

In contrast, figure 4(a) shows the nucleation and growth of the ferrite nucleus, following the higher temperature quench—as above, we have plotted the best-fit e_3 for snapshot configurations of $N = 110 \times 110$ particles at time steps of 8000, 10 000, 13 000 and $15\,000\Delta t$. The nucleus is composed of polycrystalline grains of the rhombic phase separated by large-angle grain boundaries. As time progresses, the grains rotate with respect to each other, giving rise to large non-affine distortions *even in the bulk of the nucleus*. This is reflected in the large values of χ in the bulk of the growing nucleus, figure 4(b). However, a spatial average of the instantaneous values χ and e_3 over a scale larger than the grain size gives zero for both. Similarly, a time average of the local χ and e_3 over a window corresponding to typical grain reorganization times gives zero for both. The plastic zone spreads throughout the product region causing extensive atomic rearrangements.

We now take a close-up look at the NAZs—figures 5(a) and (b) show snapshots of the atomic positions in the NAZs of

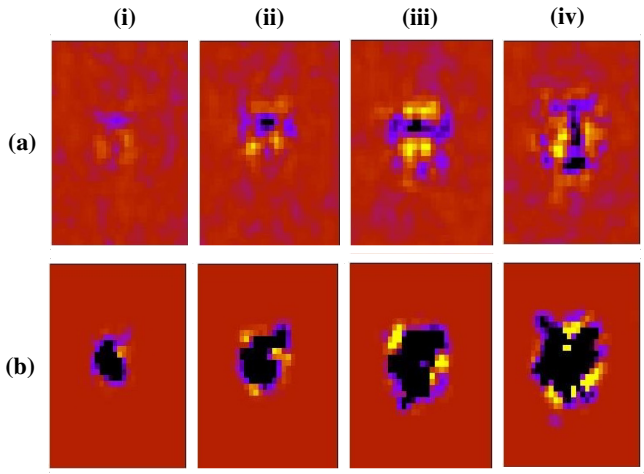

Figure 4. Best-fit affine strains and residual non-affine deformations, obtained from MD simulations for a quench at $T = 0.8$, for time slices (i) 8000, (ii) 10 000, (iii) 13 000 and (iv) 15 000Δt. Same coarse-graining as in figure 3. (a) Order parameter (shear) strain e_3: colors show e_3 from -0.3 (black) to 0.3 (yellow/white in the print edition). Note that, unlike the martensite, no clear spatial pattern in e_3 can be discerned. The local structure of the product nucleus is polycrystalline, with individual grains which coarsen with time. (b) Non-affine deformation χ: colors show χ ranging from -1 to 1. Note that non-affine regions are present throughout the interior of the nucleus, signifying extensive plastic deformation during growth.

the martensite and ferrite nucleus, respectively. It is clear that the atomic configurations in the NAZs are highly amorphous, with no clear relation to the reference parent lattice. It seems meaningless to describe NAZs in terms of a density of dislocations, since the reference state has no unique physical significance for characterizing the current state in the NAZs. Even if we were to describe the state of NAZs in terms of dislocations, the density of dislocations would be so high as to have overlapping cores, thus rendering this language inadequate. It is more reasonable to describe the NAZs in terms of fluctuations in the local density $\phi(\mathbf{r}, t) = (\rho(\mathbf{r}, t) - \rho_0)/\rho_0$, where $\rho(\mathbf{r}, t) = \sum_{n\in\Omega} \delta(\mathbf{r} - \mathbf{r}_n(t))$, and ρ_0 is the average uniform density. Indeed, in [6], we had studied the dynamics of $\phi(\mathbf{r}, t)$ in great detail and demonstrated its involvement with dynamics of transformation and microstructure selection. Here we find by explicit computation that ϕ and χ are related—localized regions with large ϕ correspond to large χ and so on.

(3) Right from its initiation, the transformation is accompanied by non-affine deformations primarily associated with NOP (here volumetric) strain. The dynamics of non-affine deformations determines the microstructure.

We will now show that NAZs are produced when the local volumetric stress exceeds a threshold value. We compute the instantaneous local stress from our MD simulations by spatially averaging the generalized virial:

$$\sigma_{ij} = \left\langle \sum_{n\in\Omega} \mathbf{F}_i \mathbf{r}_n^j \right\rangle$$

over cells Ω_M containing M particles where $1 \ll M < N$. The choice of M is dictated by the mutually competing considerations of proper averaging and obtaining information over a fine enough length scale. We have chosen $M = 100$ as a compromise between these considerations. Further, in order to obtain good statistics for any time t, we average over many independent quench runs. Thus the spatio-temporal resolution of the computed $\boldsymbol{\sigma}$ is not as high as the one for the coarse-grained strain $\mathbf{e}$.

We can now compute the local volumetric stress σ_1, affine volumetric strain e_1 and non-affine χ, averaged over the coarse-grained cell Ω_M, at different times following the quench. This is plotted in figures 6(a) and (b), where we have expressed the local stress as a fractional difference about the value of σ_1 for $e_1 = 0$, viz. the undistorted region. The σ_1–e_1 plot shows a linear elastic regime for those coarse-grained cells where the strain e_1 is small; concomitantly the non-affine χ is zero (figures 6(c) and (d)). Coarse-grained cells where e_1 is larger than a threshold show yielding

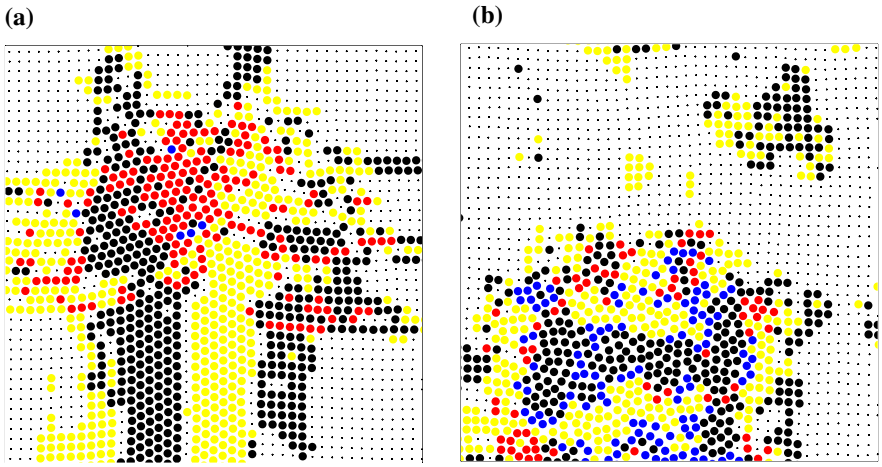

Figure 5. Close-up of a region from the nucleus (a) in martensite: corresponding to figure 3(iii) and (b) ferrite: corresponding to figure 4(iv). The color code is as follows: black dots—untransformed regions; yellow (white in the print edition) and black circles—affine regions with +ve and −ve e_3; red (light gray in the print edition) and blue (dark gray in the print edition) circles—jammed and unjammed non-affine regions. In (a) a similar non-affine region arises at the other (bottom) end of the twinned region (not shown).

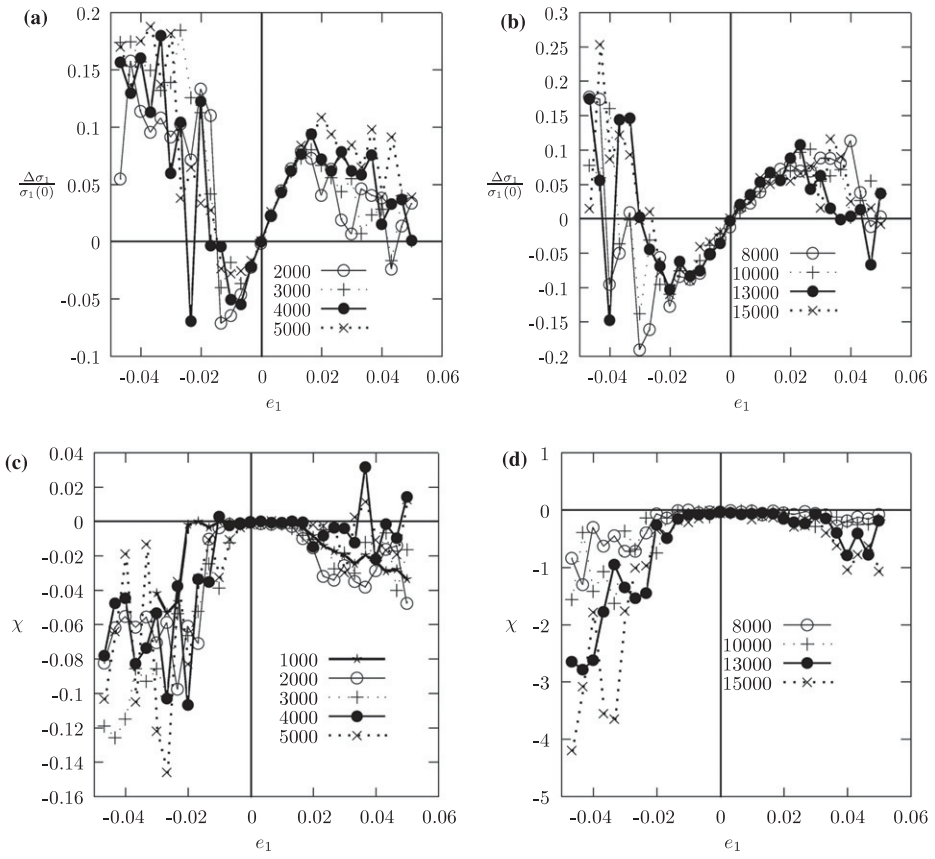

Figure 6. Local stress expressed as a fractional difference from the volumetric stress at $e_1 = 0$ ($\Delta\sigma_1/\sigma_1(0)$) plotted against the local strain at different times (symbols) obtained for the (a) quench at $T = 0.1$, averaged over 40 independent quenches, and (b) quench at $T = 0.8$, averaged over 35 independent quenches. (c) and (d) are corresponding plots of χ versus e_1. The linear Hookean regime represents the local elastic response at small local stress. Beyond a threshold, the system *yields* locally, giving rise to a nonlinear stress–strain behavior *and* simultaneously non-affine deformations $\chi \neq 0$. The regions in real space associated with this local plastic regime are identical to the NAZs. The contribution to (c) and (d) comes predominantly from unjammed regions due to the (negative) volume change which accompany the transformation.

(nonlinear and erratic σ_1–e_1) and appreciable plastic flow, $\chi \neq 0$. We have verified that these coarse-grained cells showing plastic deformation are indeed the NAZs reported above. We now focus on one coarse-grained cell and study the time development of σ_1, e_1 and χ as the transformation proceeds (figure 7). We find that, at earlier times, the strains are small and the stress–strain response is elastic. Beyond a yield stress σ_{1c}, the stress–strain relation is nonlinear, giving rise to non-affine deformations $\chi \neq 0$. Following yielding, the local stress eventually decreases, often exhibiting oscillatory behavior. We find that the threshold stresses σ_{1c}, when expressed as a fraction of the ambient stress, is only weakly dependent on temperature.

(4) Non-affine deformations are produced when the local stress crosses a threshold. The threshold stress is only weakly dependent on temperature.

These principles 1–4 highlighted above will form the basis of our construction of an elastoplastic theory for the dynamics of solid state transformations (part II). We believe they are generic, independent of the choice of potential or the nature of the transformation. In part II, we will show that the development of microstructure is crucially influenced by the dynamics of the NOP plastic strain associated with NAZs.

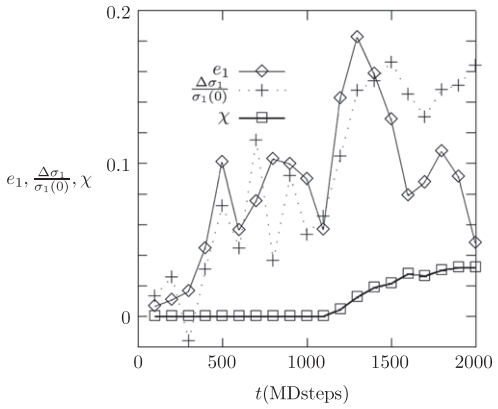

Figure 7. Time dependence of local stress $\Delta\sigma_1/\sigma_1(0)$, strain e_1 and χ near the growing nucleus within a jammed region after a quench at $T = 0.1$. Note that initially $\chi = 0$ and the stress (apart from large statistical fluctuations) is proportional to strain. When the local stress exceeds a threshold, χ begins to increase, and the stress versus strain is highly nonlinear.

4. Summary and conclusions

In this paper we have described MD simulations of a model solid, which shows that the dynamics of structural

transformation is accompanied by transient, localized regions of plasticity called NAZs. We derive a few basic characteristics for the dynamics of these NAZs and highlight their role in microstructure selection. In a companion paper we use these principles to formulate a continuum theory of microstructure selection which incorporates the dynamics of these NAZs.

Acknowledgments

We acknowledge several illuminating discussions with K Bhattacharya and A Saxena, and their useful comments on the manuscript. We thank G I Menon for a careful reading. Computer time from DST grant SP/S2/M-20/2001 and support from the Unit for Nano Science and Technology, S N Bose National Centre for Basic Sciences is gratefully acknowledged.

References

[1] Cahn R W and Haasen J 1996 *Physical Metallurgy* 4th edn (Amsterdam: Elsevier)
Kachaturyan A G 1983 *Theory of Structural Transformations in Solids* (New York: Wiley)
[2] Phillips R 2001 *Crystals, Defects and Microstructures: Modeling Across Scales* (Cambridge: Cambridge University Press)
[3] Nishiyama Z 1978 *Martensitic Transformation* (New York: Academic)
[4] Rao M and Sengupta S 1997 *Phys. Rev. Lett.* **78** 2168
Rao M and Sengupta S 1999 *Curr. Sci.* **77** 382
Sengupta S and Rao M 2003 *Physica* A **318** 251
[5] Rao M and Sengupta S 2004 *J. Phys.: Condens. Matter* **16** 7733
[6] Rao M and Sengupta S 2003 *Phys. Rev. Lett.* **91** 045502
[7] Bhadeshia H K D H 1992 *Bainite in Steels* (London: Institute of Materials)
[8] Paul A, Bhattacharya J, Sengupta S and Rao M 2008 *J. Phys.: Condens. Matter* **20** 365211
[9] Weber T A and Stillinger F H 1993 *Phys. Rev.* E **48** 4351
[10] Hatch D M, Lookman T, Saxena A and Shenoy S R 2003 *Phys. Rev.* B **68** 104105
[11] Frenkel D and Smit B 2002 *Understanding Molecular Simulations* 2nd edn (New York: Academic)
[12] Morris J R and Ho K M 1995 *Phys. Rev. Lett.* **74** 940
[13] Falk M L and Langer J S 1998 *Phys. Rev.* E **57** 7192
Langer J S 2001 *Phys. Rev.* E **64** 011504
Langer J S and Pechenik L 2003 *Phys. Rev.* E **68** 061507
[14] Edwards S F and Grinev D V 2001 *Jamming and Rheology* ed A Liu and S R Nagel (New York: Taylor and Francis)
[15] Liu A J and Nagel S R 1998 *Nature* **396** 21